J. Marine Sci. Appl., (2017) 16: 261-275
DOI: 10.1007/s11804-017-1427-5

Hydrodynamic Characteristics of Three Rows of Vertical Slotted Wall Breakwaters

Majed O. Alsaydalani[1], Mohammed A. N. Saif [1] and Medhat M. Helal[2*]

1. Civil Engineering Department, Umm Al-Qura University, Makkah 21955, Saudi Arabia
2. Department of Engineering Mathematics and Physics, Zagazig University, Zagazig 44511, Egypt

Abstract: In this study, we examine the hydrodynamic characteristics of three rows of vertical slotted wall breakwaters in which the front and middle walls are permeable and partially immersed in a water channel of constant depth, whereas the third wall is impermeable. The wave–structure interaction and flow behavior of this type of breakwater arrangement are complicated and must be analyzed before breakwaters can be appropriately designed. To study the hydrodynamic breakwater performance, we developed a mathematical model based on the eigenfunction expansion method and a least squares technique for predicting wave interaction with three rows of vertical slotted wall breakwaters. We theoretically examined the wave transmission, reflection, energy loss, wave runup, and wave force under normal regular waves. Comparisons with experimental measurements show that the mathematical model results adequately reproduce most of the important features. The results of this investigation provide a better understanding of the hydrodynamic performance of triple-row vertical slotted wall breakwaters.

Keywords: slotted breakwaters, mathematical models, transmission coefficient, reflection coefficient, energy-loss coefficient, wave runup, wave force

Article ID: 1671-9433(2017)03-0261-15

1 Introduction

Coastal protection structures can reduce coastal risks and economic losses by decreasing shoreline destruction, wave damage, and submergence. The improvement and use of coastal regions play a significant role in the national economy of many countries and these regions attract much human activity. Major concerns associated with these regions include the protection of the coastal area, harbors, and marinas by the use of the methods that have the fewest negative side effects on adjacent and neighboring shores, are environmentally friendly, and are as inexpensive as possible.

Recently, permeable breakwaters have been recommended for overcoming the weaknesses of fully protected breakwaters. These protective structures have only minor impacts on the coastal environment and neighboring beaches and provide more economical protection from waves and currents.

The many types of coastal protection approaches include artificial beaches, nourishment, breakwaters, jetties, seawalls, artificial headlands, and groins. Breakwaters are commonly used along shorelines, channel entrances, beaches, harbors, and marinas. The main function of a breakwater is to provide shore protection by controlling the allowable wave height and current velocity transmitted along the coast and inside harbors. Breakwaters are classified according to their degree of protection provided: either full or partial. Full-protection breakwaters are commonly used and are known as conventional breakwaters, although they have inherent drawbacks, including their massive size, associated environmental harm and excessive reflections, and being uneconomical in deeper water. Partial protection, or nonconventional, breakwaters, on the other hand, have been used more recently to overcome the limitations of conventional breakwaters (Tsinker, 1995).

The functional performance of the slotted breakwater is calculated by investigating wave reflection and transmission through the breakwater. Physical hydraulic tests have been conducted and many mathematical models developed to analyze wave scattering by vertical slotted breakwaters (Kriebel, 1992; Isaacson *et al*., 1998; Isaacson *et al*., 1999; Isaacson *et al*., 2000; Yong Liu and Yu-cheng Li, 2011; Elchahal *et al*., 2013; Koraim *et al*., 2014).

This study provides key information for understanding the hydraulic performance of the proposed breakwater, comprising three rows of vertical slotteyd walls, in which the front and middle walls are permeable and partially immersed in a water channel of constant depth, and the third wall is impermeable. Once the permissible transmission range for a protected area is determined, obtaining information about the wave transmission characteristics becomes critical for the selection of the appropriate configuration for the prevailing wave climate.

To meet our overall project goal, we specify the following two objectives:

1) Develop a theoretical solution using the eigenfunction expansion method and a least squares technique to estimate the wave transmission, reflection, and energy-loss characteristics of the three rows of vertical slotted wall breakwaters under regular wave conditions.

Received date: 24-Dec-2016
Accepted date: 15-Mar-2017
Foundation item: King Abdul-Aziz City for Science and Technology, General Directorate of Research Grants Programs (LGP-35-287)
***Corresponding author Email:** mmhelal@aucegypt.edu

2) Experimentally investigate these same characteristics for different wave climates and structural configurations.

Below, we summarize the methodology we used to achieve our theoretical and experimental project goals.

In section 3.1, we state our theoretical formulation and assumptions with respect to the boundary value problem of the interaction of water waves with the proposed breakwater structure. In subsection 3.1.1, we develop our mathematical formulation with respect to the boundary value problem. We divide the full domain into four regions according to each structural partition. In subsection 3.1.2, we generate an analytical solution using the eigenfunction expansion technique to obtain the velocity potential of each region. Then, we implement a least squares approach to compute the unknown expansion coefficients of the velocity potentials. Consequently, we obtain the reflection and transmission coefficients and the wave forces acting on the walls.

To examine the hydrodynamic performance of three rows of the vertical slotted wall breakwater, it was necessary to design, build, and conduct a series of experiments in a wave flume. The wave flume dimensions were 15 m in length, 0.30 m in width, and 0.45 m in depth. We installed a flap-type wave generator with a computer at one end of the flume to generate regular waves of different heights and frequencies. At the other end, we installed a wave absorber in the form of a porous beach. Further details are provided in section 3.2.

To examine the effectiveness of the proposed model, we used numerical examples. We then compared our theoretical predictions of the hydrodynamic, reflection, transmission, and energy-loss coefficients with those achieved numerically in other studies and with our own experimental research.

The authors of numerous studies have proposed configurations for slotted breakwaters to improve their performance and to study their hydrodynamic behavior in reducing incident waves. Much attention has been given to the development of different geometric shapes, along with efforts to understand the physical action of breakwaters by various numerical models.

Isaacson *et al*. (1998) presented the outlines of their numerical wave interaction calculations for a thin vertical slotted barrier extending from the water surface to some distance above the seabed, and described laboratory tests undertaken to assess their numerical model results. Comparisons of these model results with experimental measurements of the transmission, reflection, and energy-loss coefficients for a partially submerged slotted barrier showed good agreement provided certain empirical model coefficients had been suitably chosen. The authors' results showed the capability of the numerical model to account effectively for the energy dissipation by the barrier.

Isaacson *et al*. (1999) also presented numerical solutions for wave interactions with a pair of thin vertical slotted barriers. Their numerical method is based on the eigenfunction expansion method and uses a boundary condition at the surface of each barrier, which accounts for energy dissipation within the barrier.

Isaacson *et al*. (2000) then presented a theoretical analysis and an associated numerical model for assessing the performance of a breakwater consisting of a perforated front wall and an impermeable back wall. The authors based their numerical model on the eigenfunction expansion method and utilized a boundary condition at the perforated wall to account for energy dissipation. They validated the numerical model by comparing its results with those from previous numerical studies of limiting cases of a permeable seawall and of a perforated breakwater with an impermeable back wall. The relevant numerical results related to the reflection coefficient, the wave runup, and the wave force. The authors discussed the effects of porosity, breakwater geometry, and relative wavelength and described the choice of suitable required parameters to model the permeability of the breakwater.

Sahoo *et al.* (2000) studied the reflection coefficient of a single perforated wall structure. This study showed the reflection coefficient to be principally determined by the front-wall porosity and the ratio of the wave chamber width to the incident wavelength.

Zhu and Chwang (2001) presented research indicating that the hydraulic characteristics of a slotted breakwater depend mainly on the porosity—the variable describing the structure's permeability.

Suh *et al*. (2001) developed analytical models based on potential flow for predicting wave reflection from a perforated-wall caisson breakwater. Laboratory experiments were also conducted with respect to irregular waves of various significant wave heights and chamber widths. The authors concluded that the reflected wave spectrum exhibits frequency-dependent oscillatory behavior.

Brossard *et al.* (2003) conducted experimental studies on the hydrodynamic characteristics of partially immersed wave-absorbing breakwaters.

Suh *et al*. (2006, 2007) described the hydrodynamic characteristics of pile-supported vertical wall breakwaters with circular and square piles under regular and random wave conditions. The authors used the eigenfunction expansion method for the analysis and estimated the reflection, transmission, runup, and wave forces acting on the breakwater. They then extended this method to random waves.

Rageh *et al.* (2009) used physical models to study the efficiency of a breakwater consisting of caissons supported on two or three rows of piles. This efficiency was described as a function of wave transmission and reflection and wave energy dissipation coefficients.

Rageh and Koraim (2010) experimentally and theoretically studied the hydrodynamic performance of a vertical wall with a permeable lower part under normal regular waves. The authors developed a theoretical model based on the eigenfunction expansion method and the least squares technique.

A mathematical model developed by Ji and Suh (2010) computed various hydrodynamic characteristics of a multiple-row curtainwall-pile breakwater. The authors proved that the transmission coefficient decreases with an increase in relative

water depth, whereas the reflection coefficient, runup, and force exhibit the opposite trend.

Koraim (2011) theoretically and experimentally investigated the wave transmission, reflection, and energy dissipation of the double vertical wall breakwater with a permeable lower part with horizontal slots and one row with vertical slots under normal regular waves. The author developed a simple theoretical model based on an eigenfunction and found the transmission coefficient to decrease with increasing values of a dimensionless wave number, increasing wave steepness, and decreasing breakwater porosity. He concluded that the theoretical model can be used to predict the performance of slotted breakwaters and the hydrodynamic forces exerted on these structures.

Ahmed *et al*. (2011) and Ahmed and Schlenkhoff (2014) developed a numerical model based on the eigenfunction expansion method for regular linear wave interactions with single and double vertical slotted walls and nonlinear, Stokes second-order wave interactions with a single vertical slotted wall. The authors validated the numerical model by comparing its results with those of previous studies and their own experimental results. They found *f* and the coefficient of porosity ε to have significant influence on the reflection $C_{R,}$ transmission C_T, and energy losses C_L of the permeable breakwaters, whereas the influence of the added mass coefficient C_m is minimal and can be omitted for this configuration.

Koraim (2011) theoretically and experimentally studied the wave reflection, transmission, and energy dissipation of a double vertical wall with a permeable lower part under normal regular waves. The authors investigated the effect of different wave and structural parameters on hydrodynamic characteristics including the wave length, upper-part drafts, porosities, and the space between the double walls.

Liu and Li (2011) examined the hydrodynamic performance of a wave-absorbing double curtain-wall breakwater consisting of a seaward perforated wall and a shoreward impermeable wall. The authors calculated the reflection coefficient, transmission coefficient, and wave forces acting on the walls and found the obtained numerical results for limiting cases to agree very well with previous predictions for single and double partially immersed impermeable walls.

Elchahal *et al.* (2013) developed algorithms to determine the optimal shape and location of detached breakwaters in ports subject to wave disturbance and navigational constraints. Furthermore, three-dimensional Navier–Stokes equation-type numerical models have been used to study the interaction of water waves with impermeable structures (Ha *et al.*, 2013; Higuera *et al.*, 2013a).

Koraim *et al.* (2014) experimentally and theoretically studied the wave transmission, reflection, and energy dissipation of double rows of vertical piles suspending horizontal steel C-shaped bars under normal regular waves. The authors investigated different wave and structural parameters, e.g., the wave length, the C-shaped bars draft and spacing, the supporting piles diameter and spacing, and the space between the double rows. Also, they developed a theoretical model based on the eigenfunction expansion method and a least squares approach to study the hydrodynamic breakwater performance.

Liu *et al.* (2014) analytically and experimentally studied the wave motion over a submerged Jarlan-type breakwater comprising a solid rear wall and a perforated front wall. The authors generated an explanatory result utilizing matched eigenfunction expansions. The calculated results showed the submerged Jarlan-type perforated breakwater to have lower wave forces and better wave-absorbing performance. For engineering designs, they found the ideal porosity values for the front wall, the relative immersed depth of the breakwater, and the relative chamber width between the front and rear walls to be 0.1-0.2, 0.1-0.2, and 0.3-0.4, respectively.

Liu *et al.* (2016) analyzed the oblique wave interaction of perforated caisson breakwaters with perforated partition walls by deriving solutions for some special existing breakwater cases. They also validated their analytical results by comparing them with their experimental data, including reflection coefficients, wave forces, and surface amplitudes.

Vílchez *et al.* (2016) numerically calculated hydraulic performance for wave–breakwater interaction. The authors generated a characteristic friction diagram to evaluate the friction in a porous medium for different breakwater types. The results showed one friction coefficient to be sufficient for accurately calculating the friction forces. The numerical computations provided optimal reflection and transmission coefficients.

Xiao *et al.* (2016) investigated wave attenuation, wave runup, motion response, and mooring force. The authors found these four aspects to increase significantly with decreasing porosity of the breakwater. In addition, they found wave attenuation and wave runup to be frequency-dependent with multiple peaks and incident wave amplitude to significantly affect the energy dissipation of short waves.

Ji *et al.* (2016) proposed four types of floating breakwaters and found the mesh cage to be the best type for wave attenuation, the motion responses and mooring forces of the porous type to be the smallest, and the porous structure based on a mesh cage to be most promising.

Gayen and Mondal (2016) investigated the wave interaction associated with two symmetric inclined porous plates and computed the physical quantities using the solutions of two hypersingular integral equations of the second kind. The authors also numerically estimated the reflection and transmission coefficients, amplitudes of the hydrodynamic forces and moments, and the wave dissipation coefficient.

Elbisy *et al.* (2016) studied the hydrodynamic performance of multiple-row vertical slotted breakwaters and constructed a mathematical technique based on the eigenfunction and least squares methods. The authors compared their results with their experimental data regarding the reflection, transmission, and dissipation coefficients as a function of k_0h. They found

the mathematical model to satisfy most of the important features in double- and triple-row breakwaters.

2 Research methodology

2.1 Theoretical formulation and assumptions

2.1.1 Mathematical formulation

Let us consider the triple-row vertical slotted wall breakwater diagrammed in Fig. 1, in which the front and middle walls are permeable and partially immersed in a water channel of constant depth h, whereas the third wall is impermeable. In the figure, the draft of the breakwater d is constant and δ is the thickness of the wall. The chamber width (the separation between the front and rear walls) is B (Fig. 1). The perforated breakwater is subject to normally incident regular waves of height H and wave length L. We define a Cartesian coordinate system (x and z) with the positive x directed from left to right from a point on the first wall and the vertical coordinate z measured vertically upward from the water line.

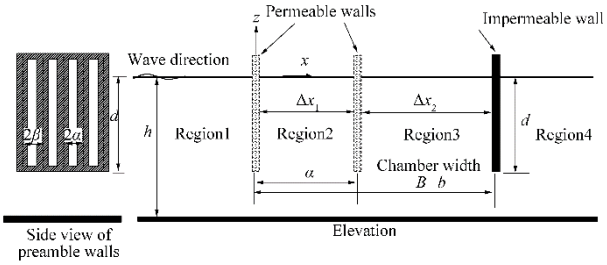

Fig. 1 Schematic and definitions of triple vertical slotted wall breakwater

The water wave problem has a free surface boundary that moves with the water particle velocity. This velocity is one of the unknown variables. Therefore, prior to computation, the position of the free surface boundary is also an unknown variable. The fluid domain is divided into four regions by the three walls. Assuming an incompressible fluid and irrotational flow motion, a velocity potential exists that satisfies the Laplace equation. For monochromatic incident waves with angular frequency ω and time t, we obtain the following boundary value problem for the velocity potential $\Phi(x, z, t)$ in each region:

$$\Phi(x,z,t)=\mathrm{Re}\left\{\phi(x,z)\mathrm{e}^{-\mathrm{i}\omega t}\right\} \tag{1}$$

where Re[ ] denotes the real part of the argument, ϕ denotes the spatial velocity potential, and $\mathrm{i}=\sqrt{-1}$. Assuming an incompressible fluid and irrotational flow motion, the velocity potential satisfies the Laplace equation. We obtain the following boundary value problem for the spatial velocity in each region:

$$\frac{\partial^2\phi_j}{\partial x^2}+\frac{\partial^2\phi_j}{\partial z^2}=0,\quad \text{for}\quad j=1,2,3,4 \tag{2}$$

where the subscript j represents variables in the region j. These potentials must also satisfy appropriate boundary conditions on the free surface, as follows:

$$\frac{\partial\phi_j}{\partial z}-\frac{\omega^2}{g}\phi_j=0,\quad \text{at } z=0,\quad j=1,2,3,4 \tag{3}$$

$$\frac{\partial\phi_j}{\partial z}=0,\quad \text{at } z=-h,\quad j=1,2,3,4 \tag{4}$$

$$\lim_{x\to-\infty}\left(\frac{\partial\phi_R}{\partial z}+\mathrm{i}k_0\phi_R\right)=0 \tag{5}$$

$$\lim_{x\to+\infty}\left(\frac{\partial\phi_4}{\partial z}-\mathrm{i}k_0\phi_4\right)=0 \tag{6}$$

where k_0 is the incident wave number, g is the gravitational acceleration, and ϕ_R is the velocity potential of the reflected waves. Moreover, we obtain the reduced velocity potentials ϕ using the eigenfunction expansion method used by Isaacson *et al*. (1998) and Suh *et al*. (2006). We express the velocity potentials in a series of infinite solutions. The solutions to Eq. (2) that satisfy the boundary conditions of Eqs. (3)–(6), are given by the following:

$$\phi_1=-\frac{\mathrm{i}gH}{2\omega}\left[\mathrm{e}^{-\alpha_0 x}Z_0(z)+R_0\mathrm{e}^{\alpha_0 x}Z_0(z)+\sum_{n=1}^{\infty}R_n\mathrm{e}^{\alpha_n x}Z_n(z)\right] \tag{7}$$

$$\phi_2=-\frac{\mathrm{i}gH}{2\omega}\left[\sum_{n=0}^{\infty}A_n\mathrm{e}^{-\alpha_n x}Z_n(z)+\sum_{n=0}^{\infty}C_n\mathrm{e}^{\alpha_n(x-a)}Z_n(z)\right] \tag{8}$$

$$\phi_3=-\frac{\mathrm{i}gH}{2\omega}\left[\sum_{n=0}^{\infty}B_n\mathrm{e}^{-\alpha_n(x-a)}Z_n(z)+\sum_{n=0}^{\infty}D_n\mathrm{e}^{\alpha_n(x-b)}Z_n(z)\right] \tag{9}$$

$$\phi_4=-\frac{\mathrm{i}gH}{2\omega}\left[T_0\mathrm{e}^{-\alpha_0(x-b)}Z_0(z)+\sum_{n=1}^{\infty}T_n\mathrm{e}^{-\alpha_n(x-b)}Z_n(z)\right] \tag{10}$$

where R_n, A_n, B_n, C_n, D_n, and T_n (n = 0, 1, 2, …) are the coefficients of the component waves propagating forward and backward, respectively. The wave numbers $\alpha_n=k_n, n=1,2,...$ are solutions to the first-order dispersion relation, $\omega^2=-g\,k_n\tan(k_n h)$ (Chakrabarti, 1987; Sarpkaya *et al.*, 1982), which have an infinite discrete set of real roots $\pm k_n$ for ($n\geq1$) for non-propagating evanescent waves and a pair of imaginary roots $\alpha_0=\pm\mathrm{i}k_0$ for propagating waves. Here we take the negative sign so that the propagating waves in Eqs. (7)–(10) correspond to the reflected and transmitted waves, respectively. We also take the positive roots of $n\geq1$ so that the non-propagating waves vanish exponentially with distance from the wall. In Eqs. (7)–(10), the depth-dependent functions $Z_n(z)$ (n = 0, 1, 2, …) are given by the following:

$$Z_0(z)=\frac{\cosh k_0(z+h)}{\cosh(k_0h)},\quad Z_n(z)=\frac{\cos k_n(z+h)}{\cos(k_nh)} \tag{11}$$

Equations (7)–(10) satisfy all the relevant boundaries and automatically satisfy the requirement that the horizontal velocities be matched at the breakwater. Therefore, the velocity potentials must satisfy the following boundary conditions at the interfaces of the breakwater, as follows:

$$\frac{\partial \phi_1}{\partial x}=\frac{\partial \phi_2}{\partial x}=\mathrm{i}k_0 G\left(\phi_1-\phi_2\right),\quad x=0,\quad -d\le z\le 0 \tag{12}$$

$$\frac{\partial \phi_1}{\partial x}=\frac{\partial \phi_2}{\partial x},\quad x=0,\quad -h\le z\le -d \tag{13}$$

$$\phi_1=\phi_2,\quad x=0,\quad -h\le z\le -d \tag{14}$$

$$\frac{\partial \phi_2}{\partial x}=\frac{\partial \phi_3}{\partial x}=\mathrm{i}k_0 G\left(\phi_2-\phi_3\right),\quad x=a,\quad -d\le z\le 0 \tag{15}$$

$$\frac{\partial \phi_2}{\partial x}=\frac{\partial \phi_3}{\partial x},\quad x=a,\quad -h\le z\le -d \tag{16}$$

$$\phi_2=\phi_3,\quad x=a,\quad -h\le z\le -d \tag{17}$$

$$\frac{\partial \phi_3}{\partial x}=\frac{\partial \phi_4}{\partial x}=0,\quad x=b,\quad -d\le z\le 0 \tag{18}$$

$$\frac{\partial \phi_3}{\partial x}=\frac{\partial \phi_4}{\partial x},\quad x=b,\quad -h\le z\le -d \tag{19}$$

$$\phi_3=\phi_4,\quad x=b,\quad -h\le z\le -d \tag{20}$$

Following Chwang (1983) and Yu (1995), we express G as follows:

$$G=\frac{\varepsilon}{\delta(f-\mathrm{i}s)}=|G|\mathrm{e}^{\mathrm{i}\theta},\quad 0\le\theta\le\pi/2 \tag{21}$$

where 'G' is the permeability parameter of a thin perforated wall, which is generally complex, and θ is the argument of the complex G. We note that when waves pass through a thin perforated wall, both a wave energy dissipation and a phase shift in the wave motion may occur. The energy dissipation due to the resistance effect of the wall is relevant to the real part of G. However, the phase shift due to the inertial effect of the wall is relevant to the imaginary part of G. When $|G|$ equals zero, the perforated wall reduces to an impermeable wall, whereas when $|G|$ tends toward infinity, the wall becomes entirely transparent. δ is the wall thickness and f is the friction coefficient. We denote the distance between the centers of two adjacent legs as 2β and the width of the opening between the legs as 2α. We denote the porosity of the perforated part of the wall as $\varepsilon=\alpha/\beta$ and the inertia coefficient as s, as given by the following:

$$s=1+C_m\left(\frac{1-\varepsilon}{\varepsilon}\right) \tag{22}$$

where C_m represents the added mass coefficient, which is treated as a constant. In this study, $f=2.0$ and we treated C_m as a constant ($C_m=0$), as suggested by Isaacson *et al.* (1998).

2.1.2 Analytic solution

The expressions for ϕ_j, $j=1, 2, 3, 4$ satisfy the seabed, free surface, and convection conditions, as well as the above mentioned boundary conditions for $x=x_i$. For convenience, we reduce these matching boundary conditions in Eqs. (12) - (20) as follows:

$$\frac{\partial \phi_1}{\partial x}=\frac{\partial \phi_2}{\partial x},\quad x=0 \tag{23}$$

$$\frac{\partial \phi_1}{\partial x}=\mathrm{i}k_0 G\left(\phi_1-\phi_2\right),\quad x=0,\quad -d\le z\le 0 \tag{24}$$

$$\phi_1=\phi_2,\quad x=0,\quad -h\le z\le -d \tag{25}$$

$$\frac{\partial \phi_2}{\partial x}=\frac{\partial \phi_3}{\partial x},\quad x=a \tag{26}$$

$$\frac{\partial \phi_2}{\partial x}=\mathrm{i}k_0 G\left(\phi_2-\phi_3\right),\quad x=a,\quad -d\le z\le 0 \tag{27}$$

$$\phi_2=\phi_3,\quad x=a,\quad -h\le z\le -d \tag{28}$$

$$\frac{\partial \phi_3}{\partial x}=\frac{\partial \phi_4}{\partial x},\quad x=b \tag{29}$$

$$\frac{\partial \phi_3}{\partial x}=0,\quad x=b,\quad -d\le z\le 0 \tag{30}$$

$$\phi_3=\phi_4,\quad x=b,\quad -h\le z\le -d \tag{31}$$

Substituting the expressions for the velocity potentials in Eqs. (7) and (8) into the boundary condition shown in Eq. (23) yields the following:

$$R_0=1-A_0+C_0\mathrm{e}^{-\alpha_0 a} \tag{32}$$

$$R_n=-A_n+C_n\mathrm{e}^{-\alpha_n a},\qquad n=1,2,\ldots \tag{33}$$

Substituting Eqs. (7) and (8) into the boundary condition shown in Eqs. (24) and (25), with the aid of Eqs. (32) and (33), yields the following:

$$\begin{aligned}&2\mathrm{i}k_0GZ_0+\sum_{n=0}^{\infty}\left(-2\mathrm{i}k_0G+\alpha_n\right)A_nZ_n-\\&\sum_{n=0}^{\infty}\alpha_nC_nZ_n\mathrm{e}^{-\alpha_n a}=0,\qquad -d\le z\le 0\end{aligned} \tag{34}$$

$$2Z_0-2\sum_{n=0}^{\infty}A_nZ_n=0,\qquad -h\le z\le -d \tag{35}$$

Also, substituting Eqs. (8) and (9) into the boundary condition shown in Eq. (26) yields the following:

$$\begin{aligned}&\sum_{n=0}^{\infty}A_n\mathrm{e}^{-\alpha_n a}Z_n-\sum_{n=0}^{\infty}B_nZ_n+\\&\sum_{n=0}^{\infty}C_nZ_n+\sum_{n=0}^{\infty}D_n\mathrm{e}^{\alpha_n(a-b)}Z_n=0\end{aligned} \tag{36}$$

Substituting Eqs. (8) and (9) into the boundary condition shown in Eqs. (27) and (28), with the aid of Eq. (36), yields the following:

$$\sum_{n=0}^{\infty}-\left(2\mathrm{i}k_0G+\alpha_n\right)A_n\mathrm{e}^{-\alpha_n a}Z_n+\sum_{n=0}^{\infty}\alpha_nC_nZ_n+\sum_{n=0}^{\infty}2\mathrm{i}k_0GB_nZ_n=0,\qquad -d\le z\le 0 \tag{37}$$

$$2\sum_{n=0}^{\infty}A_n\mathrm{e}^{-\alpha_n a}Z_n-2\sum_{n=0}^{\infty}B_nZ_n=0,\qquad -h\le z\le -d \tag{38}$$

Finally, substituting Eqs. (9) and (10) into the boundary condition shown in Eq. (29) yields the following:

$$-B_n\,\mathrm{e}^{-\alpha_n(b-a)}+D_n+T_n=0,\qquad n=0,1,2,... \tag{39}$$

Substituting Eqs. (9) and (10) into the boundary condition shown in Eqs. (30) and (31) yields the following:

$$\sum_{n=0}^{\infty}-B_n\,\mathrm{e}^{-\alpha_n(b-a)}Z_n+\sum_{n=0}^{\infty}D_nZ_n=0,\qquad -d\le z\le 0 \tag{40}$$

$$2\sum_{n=0}^{\infty}D_nZ_n=0,\qquad -h\le z\le -d \tag{41}$$

Equations (34), (35), (36), (37), (38), (40), and (41) are known as series relations, as described by Dalrymple and Martin (1990), and are solved for the values of the coefficients by the least squares method. Every condition specifies the potential along the z-axis such that the function $S(z)$ denotes the boundary condition of the wall as follows:

$$S_1^{-d\le z\le 0}(z)=2\mathrm{i}k_0GZ_0+\sum_{n=0}^{\infty}\left(-2\mathrm{i}k_0G+\alpha_n\right)A_nZ_n-\sum_{n=0}^{\infty}\alpha_nC_nZ_n\,\mathrm{e}^{-\alpha_n a} \tag{42}$$

$$S_1^{-h\le z\le -d}(z)=2Z_0-2\sum_{n=0}^{\infty}A_nZ_n \tag{43}$$

$$S_2^{-h\le z\le 0}(z)=\sum_{n=0}^{\infty}A_n\,\mathrm{e}^{-\alpha_n a}Z_n-\sum_{n=0}^{\infty}B_nZ_n+\sum_{n=0}^{\infty}C_nZ_n+\sum_{n=0}^{\infty}D_n\mathrm{e}^{\alpha_n(a-b)}Z_n \tag{44}$$

$$S_3^{-d\le z\le 0}(z)=\sum_{n=0}^{\infty}-\left(2\mathrm{i}k_0G+\alpha_n\right)A_n\mathrm{e}^{-\alpha_n a}Z_n+\sum_{n=0}^{\infty}\alpha_nC_nZ_n+\sum_{n=0}^{\infty}2\mathrm{i}k_0GB_nZ_n \tag{45}$$

$$S_3^{-h\le z\le -d}(z)=2\sum_{n=0}^{\infty}A_n\mathrm{e}^{-\alpha_n a}Z_n-2\sum_{n=0}^{\infty}B_nZ_n \tag{46}$$

$$S_4^{-d\le z\le 0}(z)=\sum_{n=0}^{\infty}-B_n\,\mathrm{e}^{-\alpha_n(b-a)}Z_n+\sum_{n=0}^{\infty}D_nZ_n \tag{47}$$

$$S_4^{-h\le z\le -d}(z)=2\sum_{n=0}^{\infty}D_nZ_n \tag{48}$$

2.1.3 Least squares technique

The least squares technique, as suggested by Dalrymple and Martin (1990), may be used to determine the six coefficients, and requires that:

$$\int_{-h}^{0}\left|S(\mathrm{z})\right|^2\,\mathrm{d}z=\text{minimum},\qquad -h<z<0 \tag{49}$$

Minimizing these integrals with respect to each coefficient, for example A_m, leads to the following:

$$\int_{-h}^{0}S^*(\mathrm{z})\frac{\partial S(\mathrm{z})}{\partial A_m}\,\mathrm{d}z=0,\qquad m=0,1,2,..., \tag{50}$$

where $S^*(\mathrm{z})$ is the complex conjugate of $S(\mathrm{z})$. Then, integrating with respect to z in Eq. (50) and truncating after N terms yields the following set of linear equations:

$$\left[\boldsymbol{a}_{1mn}\right]_{N\times N}\left[\boldsymbol{A}_n^*\right]_N+\left[\boldsymbol{a}_{2mn}\right]_{N\times N}\left[\boldsymbol{C}_n^*\right]_N=\left[\boldsymbol{a}_{3mn}\right]_{N\times N} \tag{51}$$

$$\left[\boldsymbol{b}_{1mn}\right]_{N\times N}\left[\boldsymbol{A}_n^*\right]_N+\left[\boldsymbol{b}_{2mn}\right]_{N\times N}\left[\boldsymbol{C}_n^*\right]_N+\left[\boldsymbol{b}_{3mn}\right]_{N\times N}\left[\boldsymbol{B}_n^*\right]_N+\left[\boldsymbol{b}_{4mn}\right]_{N\times N}\left[\boldsymbol{D}_n^*\right]_N=0 \tag{52}$$

$$\left[\boldsymbol{c}_{1mn}\right]_{N\times N}\left[\boldsymbol{A}_n^*\right]_N+\left[\boldsymbol{c}_{2mn}\right]_{N\times N}\left[\boldsymbol{C}_n^*\right]_N+\left[\boldsymbol{c}_{3mn}\right]_{N\times N}\left[\boldsymbol{B}_n^*\right]_N=0 \tag{53}$$

$$\left[\boldsymbol{d}_{1mn}\right]_{N\times N}\left[\boldsymbol{B}_n^*\right]_N+\left[\boldsymbol{d}_{2mn}\right]_{N\times N}\left[\boldsymbol{D}_n^*\right]_N=0 \tag{54}$$

where

$$a_{1mn}=\left(-2\mathrm{i}k_0G+\alpha_m\right)\left(2\mathrm{i}k_0G^*+\alpha_n^*\right)\int_{-d}^{0}Z_nZ_m\,\mathrm{d}z+4\int_{-h}^{-d}Z_nZ_m\,\mathrm{d}z \tag{55}$$

$$a_{2mn}=\left(-2\mathrm{i}k_0G+\alpha_m\right)\left(-\alpha_n^*\mathrm{e}^{-\alpha_n^* a}\right)\int_{-d}^{0}Z_nZ_m\,\mathrm{d}z \tag{56}$$

$$a_{3mn}=\left(-2\mathrm{i}k_0G+\alpha_m\right)\left(2\mathrm{i}k_0G^*\right)\int_{-d}^{0}Z_0Z_m\,\mathrm{d}z+4\int_{-h}^{-d}Z_0Z_m\,\mathrm{d}z \tag{57}$$

$$b_{1mn}=-\mathrm{e}^{-\alpha_n^* a}\int_{-h}^{0}Z_nZ_m\,\mathrm{d}z \tag{58}$$

$$b_{2mn}=-\int_{-h}^{0}Z_nZ_m\,\mathrm{d}z \tag{59}$$

$$b_{3mn}=-\int_{-h}^{0}Z_nZ_m\,\mathrm{d}z \tag{60}$$

$$b_{4mn}=-\mathrm{e}^{-\alpha_n^*(a-b)}\int_{-h}^{0}Z_nZ_m\,\mathrm{d}z \tag{61}$$

$$c_{1mn} = \alpha_m \left(2\mathrm{i}k_0 G^* - \alpha_n^*\right) \mathrm{e}^{-\alpha_n^* a} \int_{-d}^{0} Z_n Z_m \,\mathrm{d}z \tag{62}$$

$$c_{2mn} = \alpha_m \alpha_n^* \int_{-d}^{0} Z_n Z_m \,\mathrm{d}z \tag{63}$$

$$c_{3mn} = -2\mathrm{i}k_0 G^* \alpha_m \int_{-d}^{0} Z_n Z_m \,\mathrm{d}z \tag{64}$$

$$d_{1mn} = -\mathrm{e}^{-\alpha_n^*(a-b)} \int_{-d}^{0} Z_n Z_m \,\mathrm{d}z \tag{65}$$

$$d_{2mn} = \int_{-d}^{0} Z_n Z_m \,\mathrm{d}z + 4\int_{-h}^{-d} Z_n Z_m \,\mathrm{d}z \tag{66}$$

2.1.4 Calculation of the reflection, transmission, energy-loss coefficients, and wave forces

We can obtain the unknown coefficients A_n^*, B_n^*, C_n^*, and D_n^* by solving the linear Eqs. (51)–(54). Subsequently, we determine all the unknown expansion coefficients in the velocity potentials. We note that the first part at the right-hand side of Eq. (7) denotes incident waves propagating in the positive x-direction, the second part denotes reflected waves from the break water, and the third part denotes a series of evanescent modes decaying in the negative *x*-direction. In addition, the first part at the right-hand of Eq. (10) denotes transmitted waves propagating in the positive *x*-direction and the second part denotes a series of evanescent modes decaying in the positive *x*-direction. Once the wave potentials are calculated, we can obtain various engineering wave properties. We define the real reflection coefficient C_R as the ratio of the reflected wave height to the incident wave height as follows:

$$C_R = |R_0| \tag{67}$$

We define the real transmission coefficients C_T as the ratio of the transmitted wave height to the incident wave height, as follows:

$$C_T = |T_0| \tag{68}$$

We can calculate the energy-loss coefficient C_L as follows:

$$C_L = \sqrt{1 - C_R^2 - C_T^2} \tag{69}$$

and when $|G|$ tends toward infinity or equals zero, this energy-loss coefficient is zero.

We can obtain the wave force acting on each wall by integrating the dynamic pressure along the structure. The magnitude of the horizontal wave force on the unit width of the front wall F_f is as follows:

$$F_f = \mathrm{i}\rho\omega \int_{-d}^{0} \left(\phi_1 - \phi_2\right)\Big|_{x=0} \,\mathrm{d}z = \frac{\rho\omega}{k_0 G} \int_{-d}^{0} \frac{\partial \phi_1}{\partial x}\Big|_{x=0} \,\mathrm{d}z \tag{70}$$

$$= \frac{\rho g H}{2\mathrm{i}k_0 G}\left[(R_0 + 1)\frac{\sinh(k_0 h) - \sinh k_0(h-d)}{\mathrm{i}k_0 \cosh(k_0 h)} + \sum_{n=1}^{\infty} R_n \frac{\sin(k_n h) - \sin k_n (h-d)}{\mathrm{i}k_n \cos(k_n h)}\right]. \tag{71}$$

The magnitude of the horizontal wave force on the unit width of the rear wall F_r is as follows:

$$F_r = \mathrm{i}\rho\omega \int_{-d}^{0} \left(\phi_3 - \phi_4\right)\Big|_{x=b} \,\mathrm{d}z \tag{72}$$

$$F_r = \frac{\rho g H}{2}\left[-T_0 \frac{\sinh(k_0 h) - \sinh k_0(h-d)}{k_0 \cosh(k_0 h)} + \sum_{n=1}^{\infty}\left(2D_n - T_n\right)\frac{\sin(k_n h) - \sin k_n (h-d)}{k_n \cos(k_n h)}\right] \tag{73}$$

We define the dimensionless wave forces C_{Ff} and C_{Fr} on the front and rear walls as follows:

$$C_{Ff} = \frac{|F_f|}{\rho g H h} \tag{74}$$

$$C_{Fr} = \frac{|F_r|}{\rho g H h} \tag{75}$$

2.2 Experimental setup and measurements

We conducted the experiments in the hydraulics laboratory wave flume of the Civil Engineering Department at Umm Al-Qura University, Saudi Arabia. The proposed breakwater contained a partially immersed vertical wall close to the free surface. In hydraulic model tests of sea waves, typically, the viscosity and surface tension of water do not play a significant controlling role, and the inertia and gravity forces are considered to be the predominant governing forces.

In this series of experiments in the wave flume, we examined the hydrodynamic wave absorption performance of three rows of vertical slotted wall breakwaters. The wave flume dimensions, as shown in Fig. 2, were 15 m in length, 0.30 m in width, and 0.45 m in depth. We installed a flap-type wave generator at one end of the flume to generate regular waves of different heights and frequencies, and a wave absorber at the other end in the form of a porous beach. We conducted the experiments at a constant water depth (h) of 30 cm and generated regular waves with different wave periods (T = 0.5 to 2 s). During the experiments, we used various curtain-wall arrangements, spaces between rows, and porosities. We placed the first vertical wall to be tested at the middle of the wave flume, fixed the space between the first and third walls as $x_3 - x_1 = 2h$, and varied the location of the second wall such that Δx_1 was 0.5h, 1.0h, and 1.5h.

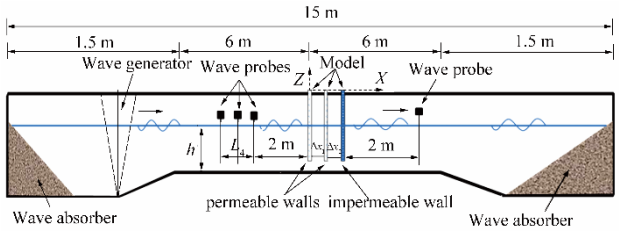

Fig. 2 Schematics diagram of the experimental setup

We constructed the vertical panels of the proposed breakwater models with a width of 0.025 m and thickness of 0.025 m. We fixed the porosity of the slotted walls at $\varepsilon = 0.5$ and fabricated the models from aluminum.

For testing purposes, we measured the water surface with four wave probes, three of which we kept at a distance of about the longest wave length from the front of the model to the second wall**.** We adjusted the spacing between the first three probes for each wave period to calculate the reflection coefficient according to the three-probe method of Mansard and Funke (1980)**.** We used three wave probes to reduce the amplitude and phase measurement errors (Mansard and Funke, 1980). We measured wave transmission with the wave probe at the rear side of the model at a distance of 2.0 m from the model.

To measure the coefficients of reflection (C_R), transmission (C_T), and dimensionless runup (R_u/H), where R_u is the runup height and H is the wave height, we used five different wave periods (T = 0.50, 0.57, 0.67, 0.80, 1.00 s). Table 1 shows the measured incident wave heights, the reflection and transmission coefficients, and the runup on the first wall of the triple vertical slotted wall breakwater.

3 Results and discussion

We computed the numerical results for the triple vertical slotted wall breakwater and compared these with our experimental results with respect to regular waves, a fixed water depth h, and a constant porosity ε for the permeable part. We varied the spacing of the second wall with respect to the first and third walls in the experiments. We present and discuss the results below.

We determined the wave interactions for the triple vertical slotted wall breakwater by its reflection, transmission, and energy-loss characteristics. We quantified the energy of the reflected waves from the first permeable wall in terms of its reflection coefficient C_R, which we defined as the ratio of the reflected wave height to the incident wave height. A C_R value of one corresponds to total reflection and zero corresponds to either total wave transmission or total wave absorption. We quantified the energy of the waves transmitted through the breakwater in terms of the transmission coefficient C_T. The energy loss through the permeable part corresponds to the difference in the energy of the incident wave and the sum of the energy of the reflected and transmitted waves. We express the energy-loss coefficient C_L as follows:

$$C_L = 1 - C_R^2 - C_T^2 \tag{76}$$

We express the wave runup on the upwave side of the first row of the breakwater as follows:

$$R_u = \frac{H}{2}\left[1 + R_0 + \frac{1}{\cosh(k_0 h)}\sum_{n=1}^{\infty} R_n \cos(k_n h)\right] \tag{77}$$

3.1 Comparisons with Porter and Evans (1995)

To validated our proposed mathematical model, we compared its results for limiting cases with the results of Porter and Evans (1995). Figure 3 shows the transmission and reflection coefficients for a triple vertical slotted wall breakwater as a function of dk_0 (Fig. 3). When $|G|$ tends to infinity, the front and second walls vanish so the three walls reduce to a single impermeable wall, as shown in Fig. 3 by Porter and Evans (1995). We can see from this figure that the agreements are acceptable between the results of our study and those of Porter and Evans (1995) at k_0h=1.5, d/h=0.5, and |G| = infinity.

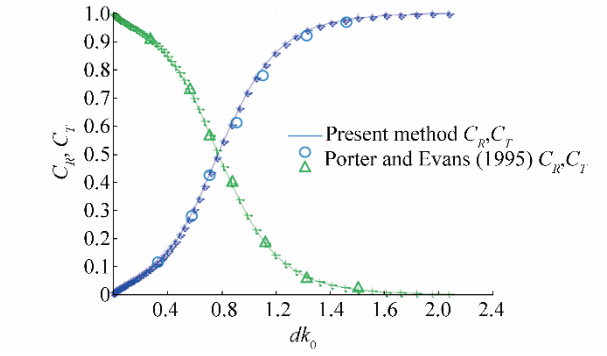

Fig. 3 Comparison of our study results with those of Porter and Evans (1995) for G=∞, k_0h=1.5, d/h=0.5

3.2 Comparisons with predicted and measured data of Isaacson *et al.* (1998)

Next, we validated our mathematical model by comparing its results with the predicted and measured results of Isaacson *et al*. (1998) with porosity = 0, such that the Isaacson *et al*. (1998) model becomes a single impermeable wall. Figure 4 shows a plot of the predicted and measured data of Isaacson *et al*. (1998) for the reflection coefficient C_R and transmission coefficient C_T, respectively, and those of our study model. In this figure, we plotted C_R and C_T as a function of dk_0, and we can see that the results obtained by our model agree approximately with the predicted and measured results of Isaacson *et al*. (1998).

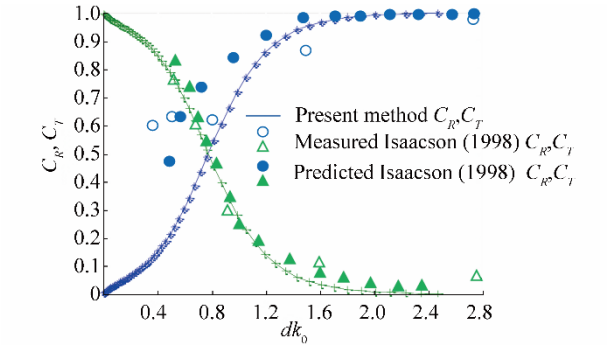

Fig. 4 Comparison of our study results with the predicted and measured results of Isaacson (1998) for $G = \infty$, $k_0h = 1.5$, $d/h = 0.5$

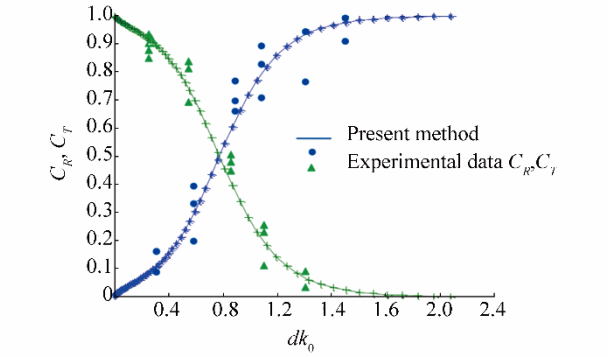

Fig. 5 Comparison of our study results and the experimental data for $G = \infty$, $k_0h = 1.5$, $d/h = 0.5$

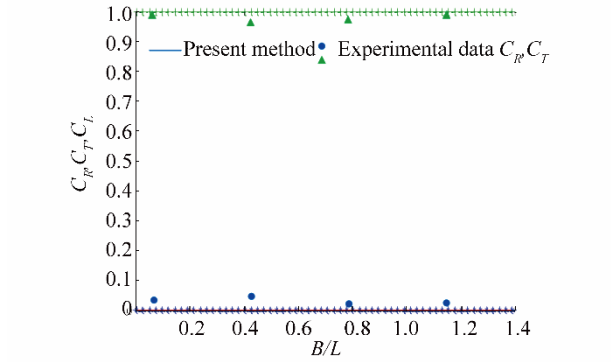

(a) $d/h = 0$

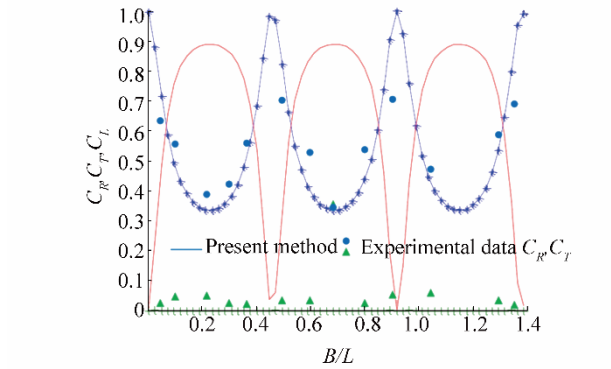

(b) $d/h = 1.0$

Fig. 6 Effects of d/h on C_R and C_T: $k_0h = 1.6$, $G = 0.5\ e^{0i}$, $\Delta x_1 = 0.5d$, and $\Delta x_2 = 0.5d$

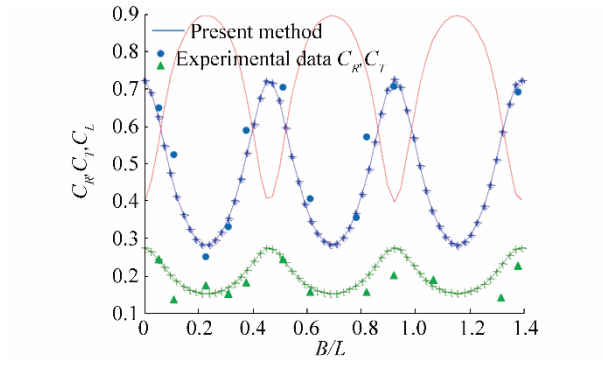

(a) $G = 0.5e^{0i}$

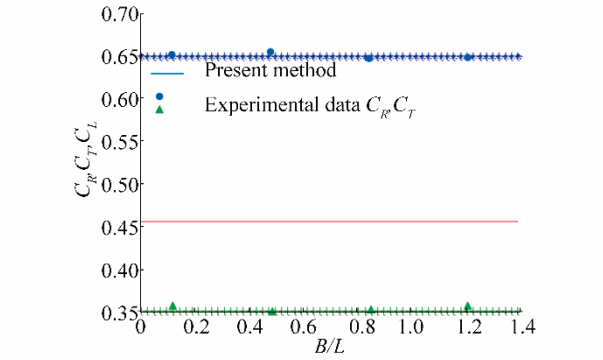

(b) $G = \infty$

Fig. 7 Effects of $|G|$ on C_R and C_T: $k_0h = 1.6$, $d/h = 0.5$, and $\Delta x_1 = 0.5d$; $\Delta x_2 = 0.5d$

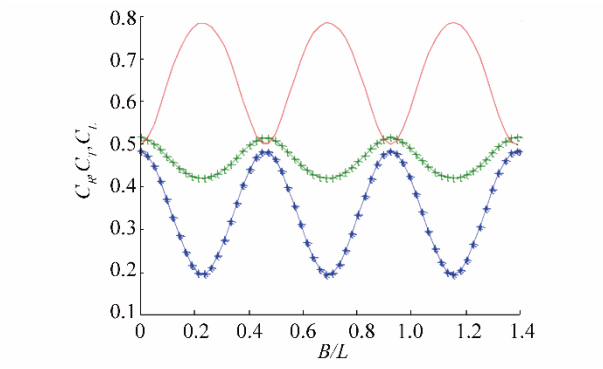

(a) $x_1 = 0.5d$, $x_2 = 1.5d$

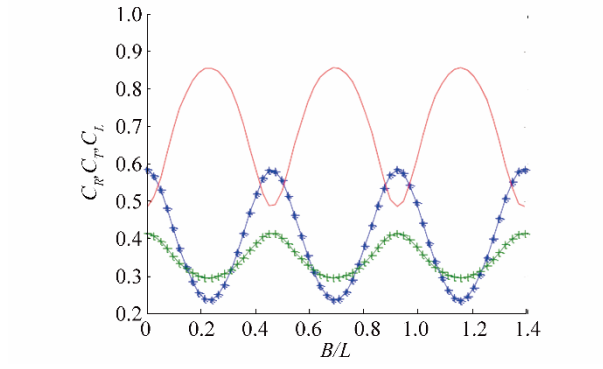

(b) $x_1 = 1.5d$, $x_2 = 0.5d$

Fig. 8 Effects of changes in the row spacing on C_R and C_T at $G = 0.5\ e^{0i}$: $k_0h = 1.6$, $d/h = 0$

Table 1 Some experimental results for triple vertical slotted wall breakwaters

$\frac{\Delta x_1}{d}$	$\frac{\Delta x_2}{d}$	$\frac{d}{h}$	T/s	H/cm	C_R	C_T	$\frac{R_u}{H}$
0.0	2.0	0.25	0.50	0.010	0.89	0.02	0.98
0.0	2.0	0.25	0.57	0.015	0.81	0.08	0.79
0.0	2.0	0.25	0.67	0.020	0.73	0.16	0.69
0.0	2.0	0.25	0.80	0.025	0.64	0.24	0.62
0.0	2.0	0.25	1.00	0.030	0.56	0.34	0.61
0.5	1.5	0.25	0.50	0.013	0.87	0.04	0.97
0.5	1.5	0.25	0.57	0.017	0.76	0.12	0.74
0.5	1.5	0.25	0.67	0.022	0.66	0.23	0.62
0.5	1.5	0.25	0.80	0.026	0.61	0.33	0.59
0.5	1.5	0.25	1.00	0.033	0.49	0.39	0.57
1.0	1.0	0.25	0.50	0.012	0.88	0.03	0.98
1.0	1.0	0.25	0.57	0.016	0.79	0.09	0.78
1.0	1.0	0.25	0.67	0.021	0.68	0.18	0.67
1.0	1.0	0.25	0.80	0.027	0.63	0.27	0.61
1.0	1.0	0.25	1.00	0.031	0.52	0.36	0.59
0.0	2.0	0.50	0.50	0.009	0.91	0.02	0.97
0.0	2.0	0.50	0.57	0.014	0.83	0.07	0.77
0.0	2.0	0.50	0.67	0.019	0.75	0.14	0.68
0.0	2.0	0.50	0.80	0.023	0.65	0.22	0.60
0.0	2.0	0.50	1.00	0.029	0.57	0.31	0.59
0.5	1.5	0.50	0.50	0.012	0.89	0.03	0.96
0.5	1.5	0.50	0.57	0.015	0.78	0.11	0.73
0.5	1.5	0.50	0.67	0.021	0.67	0.21	0.61
0.5	1.5	0.50	0.80	0.025	0.63	0.30	0.58
0.5	1.5	0.50	1.00	0.032	0.52	0.37	0.56
1.0	1.0	0.50	0.50	0.011	0.90	0.02	0.97
1.0	1.0	0.50	0.57	0.015	0.81	0.08	0.76
1.0	1.0	0.50	0.67	0.020	0.69	0.16	0.66
1.0	1.0	0.50	0.80	0.024	0.65	0.25	0.59
1.0	1.0	0.50	1.00	0.030	0.54	0.34	0.58
0.0	2.0	0.75	0.50	0.008	0.93	0.02	0.96
0.0	2.0	0.75	0.57	0.013	0.84	0.06	0.76
0.0	2.0	0.75	0.67	0.018	0.76	0.13	0.68
0.0	2.0	0.75	0.80	0.022	0.67	0.21	0.59
0.0	2.0	0.75	1.00	0.028	0.59	0.31	0.58
0.5	1.5	0.75	0.50	0.011	0.90	0.03	0.96
0.5	1.5	0.75	0.57	0.014	0.79	0.09	0.72
0.5	1.5	0.75	0.67	0.020	0.69	0.21	0.60
0.5	1.5	0.75	0.80	0.024	0.64	0.29	0.57
0.5	1.5	0.75	1.00	0.031	0.52	0.36	0.55
1.0	1.0	0.75	0.50	0.010	0.91	0.03	0.95
1.0	1.0	0.75	0.57	0.014	0.82	0.08	0.75
1.0	1.0	0.75	0.67	0.019	0.71	0.15	0.64
1.0	1.0	0.75	0.80	0.023	0.66	0.24	0.58
1.0	1.0	0.75	1.00	0.029	0.55	0.32	0.57

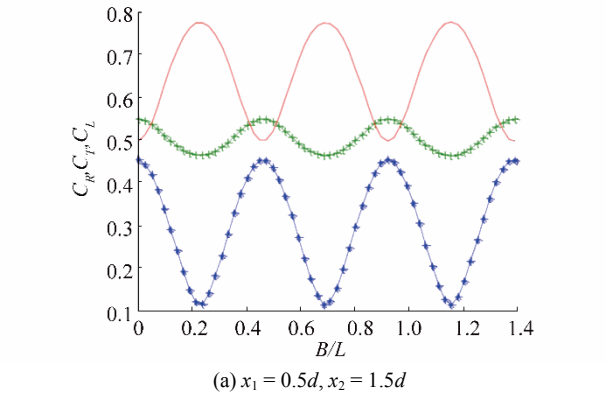

(a) $x_1 = 0.5d$, $x_2 = 1.5d$

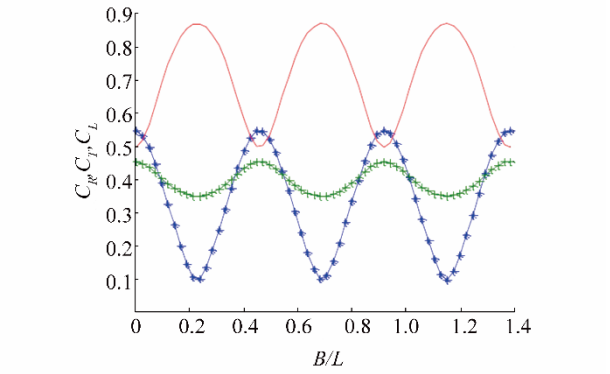

(b) $x_1 = 1.5d$, $x_2 = 0.5d$

Fig. 9 Effects of changes in the row spacing on C_R and C_T at $G = 1.0\ e^{0i}$: $k_0h = 1.6$, $d/h = 0.5$

3.3 Comparison with experimental data

We also validated our proposed mathematical model by comparing its results for limiting cases with our experimental data at $k_0h = 1.5$, $d/h = 0.5$, and $|G|$ = infinity. Fig. 5 shows the transmission and reflection coefficients for a triple vertical slotted wall breakwater as a function of dk_0. We can see from these figures that the agreements are acceptable between our model and the experimental data results.

Fig. 6 shows the effects of the relative draft d/h of the breakwater as a function of the relative wave chamber width B/L on C_R and C_T at $k_0h = 1.6$, with the energy dissipation $G = 0.5e^{0i}$ the only real part, as given in the definition of Eq. (21) and $\Delta x_1 = 0.5d$ and $\Delta x_2 = 0.5d$. In this figure, we derived the reflection and transmission coefficients from the proposed model and the experimental data, and plotted them as a function of the relative wave chamber width B/L. In general, the numerical solution satisfactorily reproduces the experimental data records. The reflection coefficient C_R increases with increasing d/h for a fixed B/L. The transmission coefficient C_T exhibits the opposite trend. We note that the model's transmission coefficient is maximum at $d/h = 0$ and minimum when d/h=1, i.e., the reflection coefficient is maximum for a wall, whereas the transmission coefficient for the same case is $C_T = 0$. It is obvious that the reflection and transmission coefficients are approximately zero and one, respectively, for $d/h = 0$.

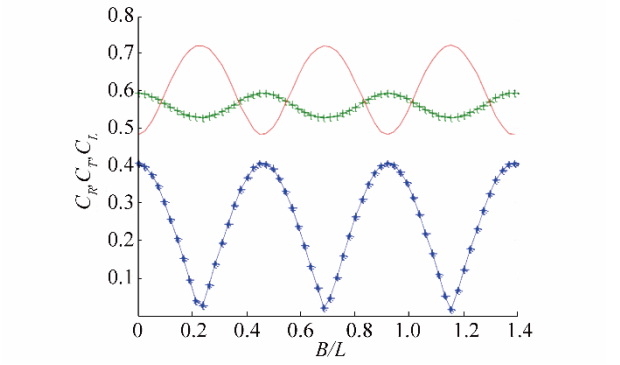

(a) $x_1 = 0.5d$, $x_2 = 1.5d$

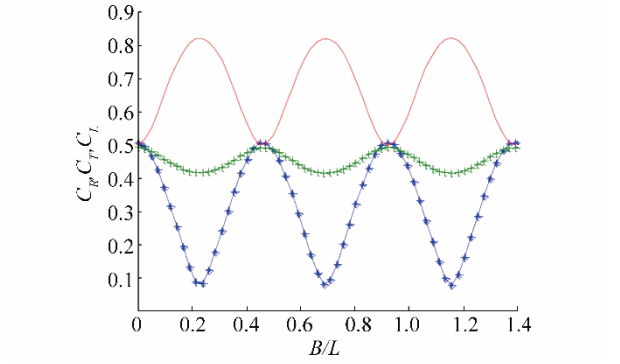

(b) $x_1 = 1.5$d, $x_2 = 0.5d$

Fig. 10 Effects of changes in the row spacing on C_R and C_T at $G = 2.0e^{0i}$: $k_0h = 1.6$, $d/h = 0.5$

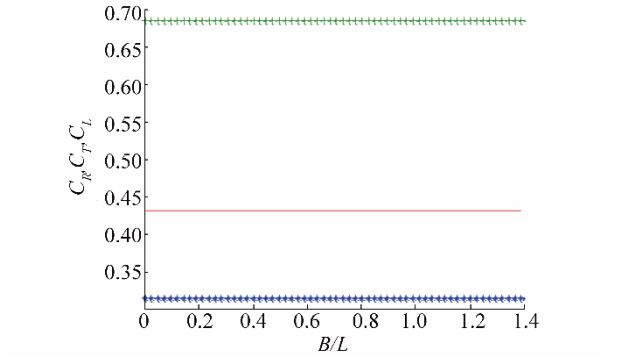

(a) $x_1 = 0.5d$, $x_2 = 1.5d$

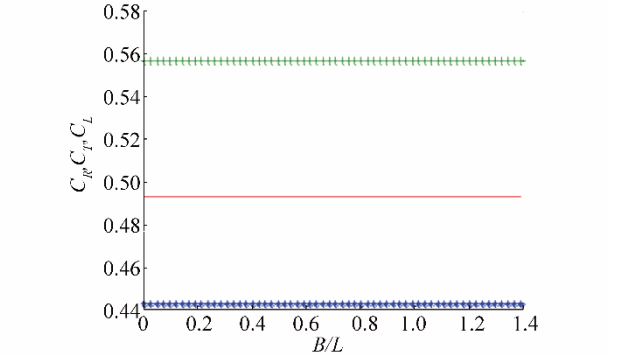

(b) $x_1 = 1.5d$, $x_2 = 0.5d$

Fig. 11 Effects of changes in the row spacing on C_R and C_T at $G = \infty$: $k_0h = 1.6$, $d/h = 0.5$

Fig. 7 shows the effects of $|G|$ of the perforated walls as a function of the relative wave chamber width B/L on C_R and C_T at $k_0h = 1.6$, $d/h = 0.5$, and $G = |G|e^{0i}$. The results follow the expected trends, wherein the reflection coefficient C_R decreases with increasing G, while the transmission coefficient C_T increases with increasing G for a fixed B/L, and the energy-loss coefficient C_L is nonzero. When $|G|$ approaches infinity, the front and middle walls disappear and then the values of both C_R and C_T are constants for different values of B/L. We validated our numerical results for the triple vertical slotted wall breakwater by comparing them with the experimental data. As shown in Fig. 7, the numerical results of our study converge with the experimental data.

Figure 8 shows the effects of changes in row spacing on C_R and C_T at $G = 0.5e^{0i}$: $k_0h = 1.6$, $d/h = 0.5$ for three different triple-row breakwater cases in which the structural parameters of the three rows are the same. We fixed the distance between the first and third rows at $\Delta x = 2.0d$ and changed the location of the second row so that in Fig. 8a, $\Delta x_1 = 0.5d$, $\Delta x_2 = 1.5d$; and for Fig. 8b $\Delta x_1 = 1.5d$, $\Delta x_2 = 0.5d$. It is interesting that the calculated transmission coefficients decrease with increasing Δx_1 for a fixed B/L, whereas the calculated reflection coefficients slowly increase with increasing Δx_1. We obtained the same results in Fig. 9 at $G = 1.0e^{0i}$, Fig. 10 at $G = 2.0e^{0i}$, and Fig. 11 at $G = \infty$. When $|G|$ approaches infinity in Fig. 11, the values of both C_R and C_T remain constant for different values of B/L. We obtained the same results in Fig. 9 at $G = 1.0e^{0i}$, Fig. 10 at $G = 2.0e^{0i}$, and Fig. 11 at $G = \infty$. When $|G|$ approaches infinity in Fig. 11, the values of both C_R and C_T remain constant for different values of B/L.

Figs. 12–14 show the effects of changes in the row spacing on C_R and C_T at $k_0h = 0.4$ for Fig. 12, $k_0h = 1.6$ for Fig. 13, $k_0h = 2.2$ in Fig. 14 when $G = 0.2/(0.4/1*.02*(9-1i))$ of Liu and Li (2011), $d/h = 0.5$ for (a) $\Delta x_1 = 0.5d$, $\Delta x_2 = 1.5d$, and (b) $\Delta x_1 = 1.5d$; $\Delta x_2 = 0.5d$. We can see that the calculated transmission coefficients decrease with increasing Δx_1 for a fixed B/L, whereas the calculated reflection coefficients slowly increase with increasing Δx_1. The oscillation of the calculated transmission and reflection coefficients both increase with increasing k_0h values.

Figs. 15 and 16 show comparisons between the predicted hydrodynamic characteristics as a function of k_0h for various distances between rows of the three walls. We fixed the distance between the first and third rows at $\Delta x = 2.0$d and changed the location of the second row so that $\Delta x_1 = 0.0d$, $\Delta x_1 = 0.5$d, $\Delta x_1 = 1.0d$, $\Delta x_1 = 1.5d$, and $\Delta x_1 = 2.0d$ with $G = 0.2/(0.4/1*.02*(9-1i))$ at $d/h = 0.8$ in Fig. 15, and $d/h = 0.2$ in Fig. 16. The dimensions of all rows were the same. We can see in Figs. 15 and 16 that C_R increases with increasing k_0h at a fixed d/h and increases with decreasing d/h at a fixed k_0h, and that C_T follows the opposite trend. We validated the numerical results for the triple vertical slotted wall breakwater by comparing its results with our experimental data and the figures show good agreement.

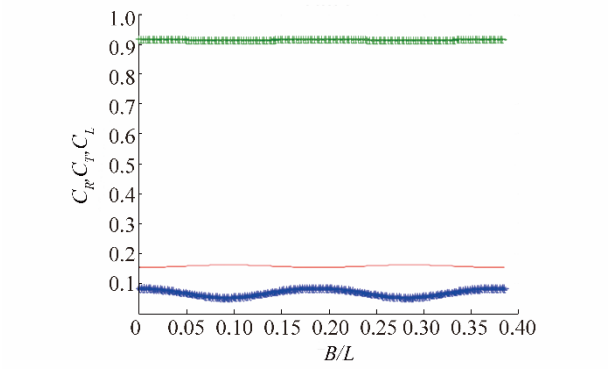

(a) $x_1 = 0.5d$, $x_2 = 1.5d$

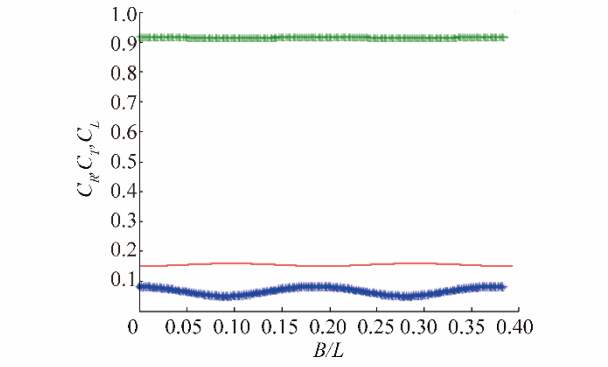

(b) $x_1 = 1.5d$, $x_2 = 0.5d$

Fig. 12 Effects of changes in the row spacing on C_R and C_T at $k_0h = 0.4$: $G = 0.2/(0.4/1*.02*(9-1i))$, $d/h = 0.5$

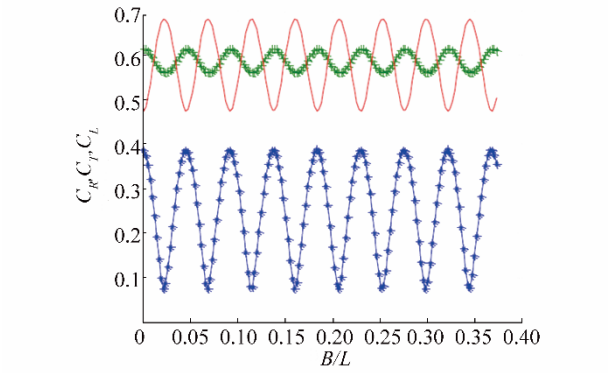

(a) $x_1 = 0.5d$, $x_2 = 1.5d$

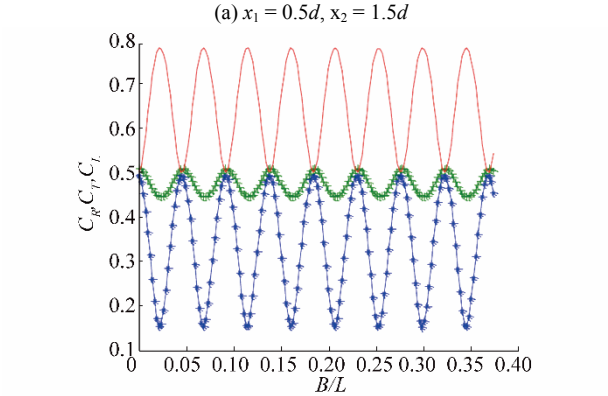

(b) $x_1 = 1.5d$, $x_2 = 0.5d$

Fig. 13 Effects of changes in the row spacing on C_R and C_T at $k_0h = 1.6$: $G = 0.2/(0.4/1*.02*(9-1i))$, $d/h = 0.5$

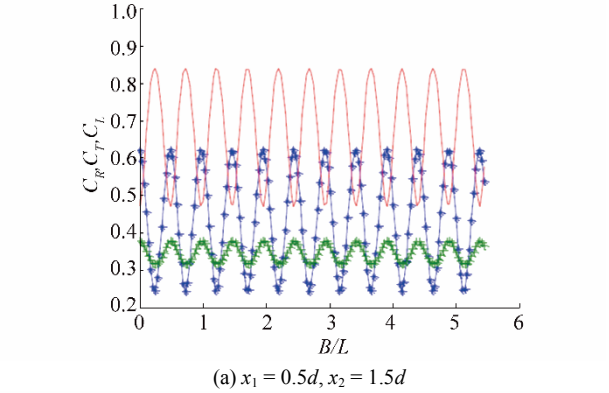

(a) $x_1 = 0.5d$, $x_2 = 1.5d$

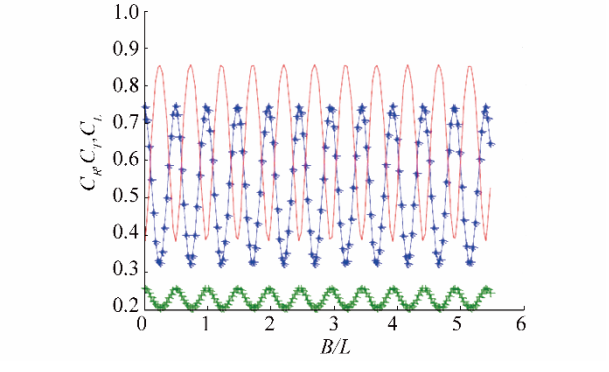

(b) $x_1 = 1.5d$, $x_2 = 0.5d$

Fig. 14 Effects of changes in the row spacing on C_R and C_T at $k_0h = 2.2$: $G = 0.2/(0.4/1*.02*(9-1i))$, $d/h = 0.5$

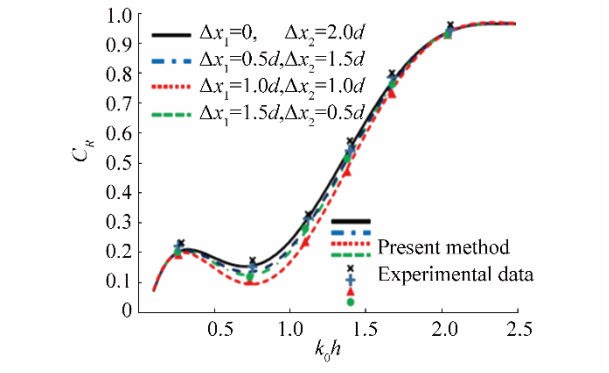

(a) Reflection coefficient C_R

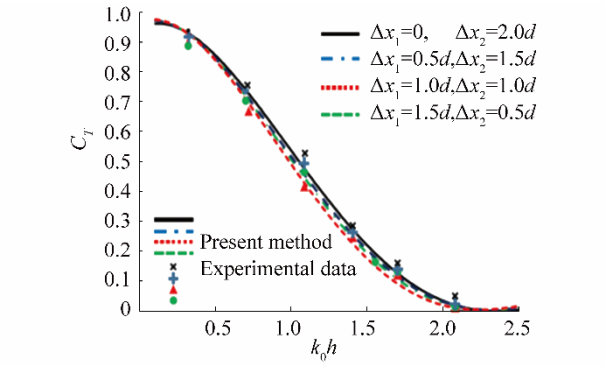

(b) Transmission coefficient C_R

Fig. 15 Predicted hydrodynamic characteristics as a function of k_0h for various distances between the rows of the triple-row walls with $G = 0.2/(0.4/1*.02*(9-1i))$, at $d/h = 0.8$

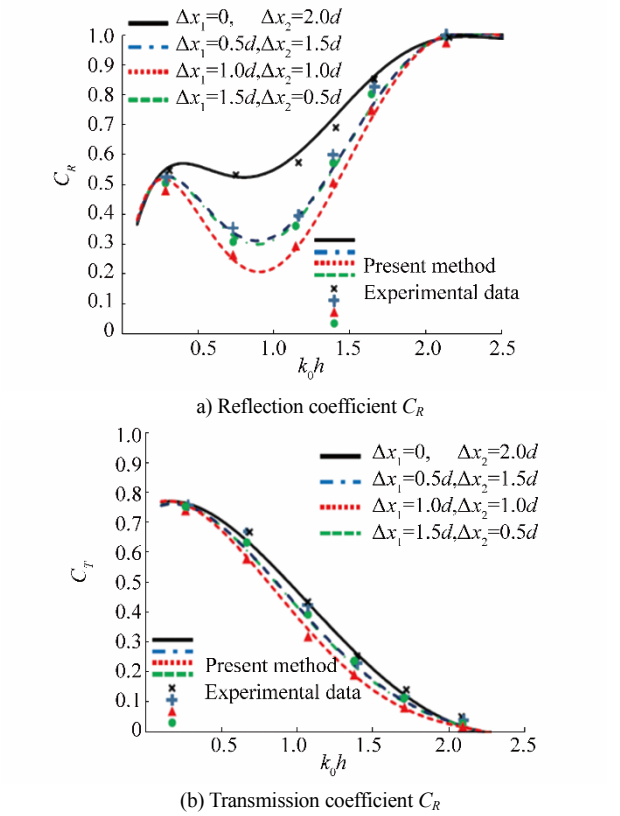

a) Reflection coefficient C_R

(b) Transmission coefficient C_R

Fig. 16 Predicted hydrodynamic characteristics as a function of k_0h for various distances between the rows of triple-row breakwaters with G = 0.2/(0.4/1*.02*(9-1i)) at d/h = 0.2

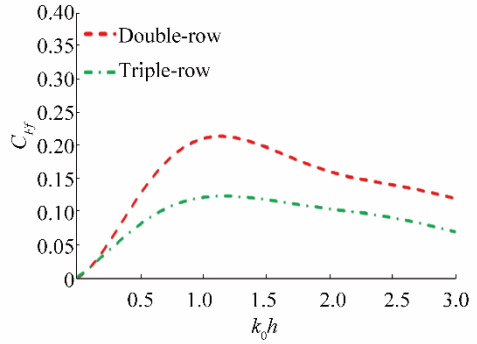

Fig. 17 Comparison of dimensionless wave force on the front wall in double-row and triple-row breakwaters as a function of k_0h, with G = 0.2/(0.4/1*.02*(9-1i)) and d/h = 0.5

Fig. 17 shows a comparison of the dimensionless wave force on the front wall of double-row and triple-row breakwaters as a function of k_0h, with G = 0.2/(0.4/1*.02*(9-1i)) and d/h = 0.5. The wave force on the front wall of the triple-row is less than that on an equivalent double-row. As expected, Fig. 18 shows that the dimensionless wave force on the rear wall of the double-row and triple-row breakwaters are considerably smaller.

Fig. 19 shows wave runup as a function of k_0h, with G = 0.2/(0.4/1*.02*(9-1i)) and d/h = 0.5 for a single-wall, double-row, and triple-row breakwater. The maximum wave runup occurs only at the first row of the breakwater, since the second and triple row values are generally smaller than those of the first row.

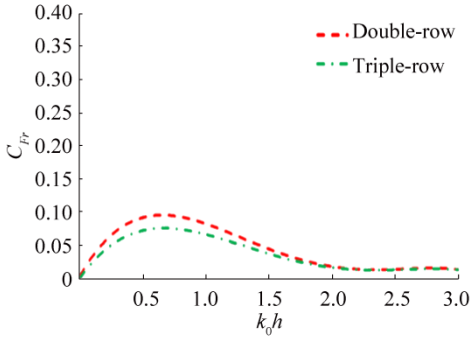

Fig. 18 Comparison of the dimensionless wave force on rear wall of double-row and triple-row breakwaters as a function of k_0h, with G = 0.2/(0.4/1*.02*(9-1i)) and d/h = 0.5

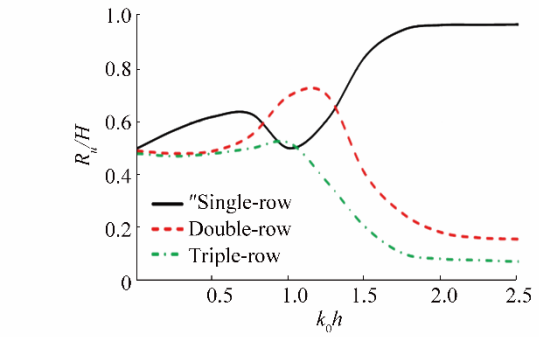

Fig. 19 Comparison of calculated runups for single-, double-, and triple-row breakwaters as a function of k_0h, with G = 0.2/(0.4/1*.02*(9-1i)) and d/h = 0.5

4 Conclusions

In this paper, we proposed a mathematical model for evaluating the hydrodynamic performance of triple vertical slotted wall breakwaters. We developed an analytical method for calculating the hydrodynamic characteristics of triple vertical slotted wall breakwaters in which the front and middle walls are permeable and partially immersed in a water channel of constant depth and the third wall is impermeable. We based our approach on the eigenfunction expansion method and a least squares technique. To validate the correctness of the proposed method, we compared its numerical results with those from laboratory tests. Specifically, we compared the C_R, C_T, and C_L coefficients for a partially submerged slotted barrier and found there to be good agreement between our numerical and experimental results, which indicates that the mathematical model can adequately reproduce most of the important features of the

experimental results.

Our numerical solutions show that the reflection coefficient C_R and transmission coefficient C_T of the breakwater are generally dependent on the relative wave chamber width B/L, the relative draft d/h, the permeability parameter of the walls G, and the incident wave number k_0h.

An increasing d/h value for a fixed B/L leads to an increase in the reflection coefficient C_R. The transmission coefficient C_T follows the opposite trend. We note that the transmission coefficient for the model is maximum at d/h=0 and minimum at d/h=1, *i.e.*, the reflection coefficient is maximum for a wall, whereas the transmission coefficient for the same case is $C_T = 0$. It is obvious that the reflection and transmission coefficients are approximately zero and one, respectively, for $d/h = 0$.

The reflection coefficient C_R decreases with increasing G, whereas the transmission coefficient C_T increases with increasing G for a fixed B/L. When |G| approaches infinity, the front and middle walls disappear and the C_R and C_T values remain constant for different values of B/L. When G increases, the calculated transmission coefficients decrease with increased spacing between the first and second rows (Δx_1) for a fixed B/L. The calculated reflection coefficients, in contrast, slowly increase with increasing Δx_1, and when $|G|$ approaches infinity, both the C_R and C_T values reamin constant for different B/L values.

When k_0h increases, the calculated transmission coefficients decrease with increasing Δx_1 for a fixed B/L, whereas the calculated reflection coefficients slowly increase with increasing Δx_1. The oscillation of the calculated transmission and reflection coefficients increase with increased k_0h values. The predicted hydrodynamic characteristics as a function of k_0h for various distances between the rows of the triple-row breakwaters show that C_R increases with increasing k_0h at a fixed d/h, and increases with decreasing d/h at a fixed k_0h. C_T follows the opposite trend.

In a comparison between the dimensionless wave force on the front wall in double-row and triple-row breakwaters as a function of k_0h, we found the wave force on the front wall of the triple-row to be less than the force on the equivalent double-row.

The study results show the wave runup to be a function of k_0h, in single-wall, double-row, and triple-row breakwaters. The maximum wave runup occurs only at the first row of the breakwater, since these values are generally smaller at the second and third rows.

Acknowledgments

The authors would like to express their gratitude and appreciation to the King Abdul-Aziz City for Science and Technology, General Directorate of Research Grants Programs for offering the research grant to support this work, under the Project number "LGP-35-287."

Acknowledgments are also due to the Civil Engineering Department, College of Engineering and Islamic Architecture, Umm Al-Qura University where the work was conducted. In addition, the authors would like to express their gratitude to the referees for their valuable comments that modified the form of the paper, and for carefully checking the manuscript.

References

Ahmed HG, Schlenkhoff A, 2014. Numerical investigation of wave interaction with double vertical slotted walls. *International Journal of Environmental, Ecological, Geological and Mining Engineering*, **8**(8), 536-543.

Ahmed HG, Schlenkhoff A, Oertel M, 2011. Stokes second-order wave interaction with vertical slotted wall breakwater, *Coastal Structures*, *Proceedings of the 6th International Conference,* Yokohama, Japan, 691-703.
DOI: 10.1142/9789814412216_0060

Brossard J, Jarno-Druaux A, Marin F, Tabet-Aoul EH, 2003. Fixed absorbing semi-immersed breakwater. *Coastal Engineering*, **49**, 25-41.
DOI: 10.1016/S0378-3839(03)00044-9

Chakrabarti SK, 1987. *Hydrodynamics of offshore structures*. Computational Mechanics Publications, Southampton, 57.

Chwang AT, 1983. A porous-wavemaker theory. *Journal of Fluid Mechanics*, **132**, 395-406.
DOI: https://doi.org/10.1017/S0022112083001676

Dalrymple RA, Martin PA, 1990. Wave diffraction through offshore breakwaters. *Journal of Waterway, Port, Coastal and Ocean Engineering*, **116**(6), 727-741.
DOI: http://dx.doi.org/10.1061/(ASCE)0733-950X(1990)116:6(727)

Elbisy MS, Mlybari EM, Helal MM, 2016. Hydrodynamic performance of multiple-row slotted breakwaters, *Journal of Marine Science and Application,* **15**(2), 123-135.
DOI: 10.1007/s11804-016-1358-6

Elchahal G, Younes R, Lafon P, 2013. Optimization of coastal structures: application on detached breakwaters in ports. *Ocean Engineering*, **63**(1), 35-43.
DOI: 10.1016/j.oceaneng.2013.01.021

Gayen R, Mondal A, 2016. Water wave interaction with two symmetric inclined permeable plates. *Ocean Engineering*, **124**, 180-191.
DOI: 10.1016/j.oceaneng.2016.07.045

Ha T, Lin P, Cho Y-S, 2013. Generation of 3D regular and irregular waves using Navier–Stokes equations model with an internal wave maker. *Coastal Engineering*, **76**, 55-67.
DOI: 10.1016/j.coastaleng.2013.01.013

Higuera P, Lara JL, Losada IJ, 2013. Realistic wave generation and active wave absorption for Navier–Stokes models: application to OpenFOAM®. *Coastal Engineering*, **71**, 102-118.
DOI: 10.1016/j.coastaleng.2012.07.002

Isaacson M, Baldwin J, Allyn N, Cowdell S, 2000. Wave interactions with perforated breakwater. *Journal of Waterway, Port, Coastal, and Ocean Engineering*, **126**, 229-235.
DOI: 10.1061/(ASCE)0733-950X(2000)126:5(229)

Isaacson M, Baldwin J, Premasiro S, Yang G, 1999. Wave interaction with double slotted barriers. *Applied Ocean Research*, **21**, 81-91.
DOI: 10.1016/S0141-1187(98)00039-X

Isaacson M, Premasiri S, Yang G, 1998. Wave interactions with vertical slotted barrier. *Journal of Waterway, Port, Coast and Ocean Engineering*, **124**, 118-126.
DOI: 10.1061/(ASCE)0733-950X(1998)124:3(118)

Ji CH, Suh KD, 2010. Wave interactions with multiple-row curtain wall-pile breakwaters. *Coastal Engineering*, **57**(5), 500-512.
DOI: 10.1016/j.coastaleng.2009.12.008

Ji CY, Chen X, Cui J, Gaidai O, 2016. Experimental study on configuration optimization of floating breakwaters. *Ocean Engineering*, **117**, 302-310.
DOI: 10.1016/j.oceaneng.2016.03.002

Koraim AS, 2011. Hydrodynamic characteristics of slotted breakwaters under regular waves. *Journal of Marine Science and Technology*, **16**, 331-342.
DOI: 10.1007/s00773-011-0126-1

Koraim AS, Iskanderb MM, Elsayed WR, 2014. Hydrodynamic performance of double rows of piles suspending horizontal C shaped bars. *Coastal engineering*, **84**, 81-96.
DOI: 10.1016/j.coastaleng.2013.11.006

Kriebel DL, 1992. Vertical wave barriers: wave transmission and wave forces. *3rd International Conference on Coastal Engineering*, 1313-1326.
DOI: https://doi.org/10.9753/icce.v23.%25p

Liu Y, Li Y, 2011. Wave interaction with a wave absorbing double curtain-wall breakwater. *Ocean Engineering*, **38**, 1237-1245.
DOI: 10.1016/j.oceaneng.2011.05.009

Liu Y, Xie L, Zhang Z, 2014. The wave motion over a submerged Jarlan-type perforated breakwater. *Acta Oceanologica Sinica*, **33**, 5, 96-102.
DOI: 10.1007/s13131-014-0471-0

Liu Y, Li Y, Teng B, 2016. Interaction between oblique waves and perforated caisson breakwaters with perforated partition walls. *European Journal of Mechanics - B/Fluids*, **56**, 143-155.
DOI: 10.1016/j.euromechflu.2015.12.001

Mansard EPD, Funke ER, 1980. The measurement of incident and reflected spectra using a least squares method. *Proceedings 17th Coastal Engineering Conference, Sydney, Australia*, 154-172.
DOI: 10.1061/9780872622647.008

Porter R, Evans DV, 1995. Complementary approximations to wave scattering by vertical barriers. *Journal of Fluid Mechanics*, **294**, 155-180.
DOI: 10.1017/S0022112095002849

Rageh OS, Koraim AS, 2010. Hydraulic performance of vertical walls with horizontal slots used as breakwater. *Coastal Engineering*, **57**, 745-756.
DOI: 10.1016/j.coastaleng.2010.03.005

Rageh OS, Koraim AS, Salem TN, 2009. Hydrodynamic efficiency of partially immersed caissons supported on piles. *Ocean Engineering*, **36**, 1112-1118.
DOI: 10.1016/j.oceaneng.2009.06.009

Sahoo T, Lee MM, Chwang AT, 2000. Trapping and generation of waves by vertical porous structures. *Journal of Engineering Mechanics, ASCE* **126**(10), 1074-1082.
DOI: 10.1061/(ASCE)0733-9399(2000)126:10(1074)

Sarpkaya T, Isaacson M, Wehausen JV, 1982. Mechanics of wave forces on offshore structures, *Journal of Applied Mechanics*, **49**(2), 466-467.
DOI:10.1115/1.3162189

Suh KD, Jung HY, Pyun CK, 2007. Wave reflection and transmission by curtain wall-pile breakwaters using circular piles. *Ocean Engineering*, **34**, 2100-2106.
DOI: 10.1016/j.oceaneng.2007.02.007

Suh KD, Park WS, Park BS, 2001. Separation of incident and reflected waves in wave-current flumes. *Coastal Engineering*, **43**, 149-159.
DOI: 10.1016/S0378-3839(01)00011-4

Suh KD, Shin S, Cox DT, 2006. Hydrodynamic characteristics of pile-supported vertical wall breakwaters. *Journal of Waterway, Port, Coast and Ocean Engineering*, **132**, 83-96.
DOI: 10.1061/(ASCE)0733-950X(2006)132:2(83)

Tsinker G, 1995. *Marine structures engineering: specialized applications*. Chapman and Hall, 568.

Vílchez M, Clavero M, Lara JL, Losada MA, 2016. A characteristic friction diagram for the numerical quantification of the hydraulic performance of different breakwater types, *Coastal Engineering*, **114**, 86-98.
DOI: 10.1016/j.coastaleng.2016.03.006

Xiao LF, Kou YF, Tao LB, Yang LJ, 2016. Comparative study of hydrodynamic performances of breakwaters with double-layered perforated walls attached to ring-shaped very large floating structures. *Ocean Engineering*, **111**, 279-291.
DOI: 10.1016/j.oceaneng.2015.11.007

Yu X, 1995. Diffraction of water waves by porous breakwater. *J. of Waterway, Port, Coastal and Ocean Engineering*, **121**, 6, 275-282.
DOI: 10.1061/(ASCE)0733-950X(1995)121:6(275)

Zhu ST, Chwang AT, 2001. Investigations on the reflection behaviour of a slotted seawall. *Coastal Engineering*, **43**, 93-104.
DOI: 10.1016/S0378-3839(01)00008-4